ORNL/TM-2023/2875

Investigation of Coincidence Counting for Improving Minimal Detectable Activity of ^{110m}Ag in Single Particle Gamma Analysis

K. Callie Goetz
Darren J. Skitt
James M. Allmond
Tim J. Gray
John D. Hunn
Tyler J. Gerczak

March 2023

Approved for public release.
Distribution is unlimited.

OAK RIDGE National Laboratory

ORNL IS MANAGED BY UT-BATTELLE LLC FOR THE US DEPARTMENT OF ENERGY

ORNL/TM-2023/2875

Nuclear Energy and Fuel Cycle Division

INVESTIGATION OF COINCIDENCE COUNTING FOR IMPROVING MINIMAL DETECTABLE ACTIVITY OF ^{110m}Ag IN SINGLE PARTICLE GAMMA ANALYSIS

K. Callie Goetz
Darren J. Skitt
James M. Allmond
Tim J. Gray
John D. Hunn
Tyler J. Gerczak

March 2023

Prepared by
OAK RIDGE NATIONAL LABORATORY
Oak Ridge, TN 37831
managed by
UT-BATTELLE LLC
for the
US DEPARTMENT OF ENERGY
under contract DE-AC05-00OR22725

CONTENTS

LIST OF FIGURES

LIST OF TABLES

ABBREVIATIONS

AGR	Advanced Gas Reactor (Fuel Development and Qualification Program)
AGR-2	second AGR irradiation
AGR-5/6/7	fourth AGR irradiation
BGO	bismuth germanium oxide (bismuth germanate)
EOI	end of irradiation
ENSDF	Evaluated Nuclear Structure Data File
FDSi	FRIB Decay Station initiator
FIMA	fissions per initial metal atom
FRIB	Facility for Rare Isotope Beams (FRIB)
HPGe	high-purity germanium
IMGA	Irradiated Microsphere Gamma Analyzer
MDA	minimum detectable activity
NNDC	National Nuclear Data Center
ORNL	Oak Ridge National Laboratory
PIE	post-irradiation examination
TAVA	time-averaged, volume-averaged (irradiation temperature)
TRISO	tristructural isotropic (coated particles)

ACKNOWLEDGMENTS

This work was sponsored by the US Department of Energy Office of Nuclear Energy, Advanced Reactor Technologies as part of the Advanced Gas Reactor Fuel Development and Qualification Program.

1. BACKGROUND

Post-irradiation examination (PIE) of fuel particles from the fourth Advanced Gas Reactor Fuel Development and Qualification (AGR) Program irradiation (AGR-5/6/7) is being performed at Oak Ridge National Laboratory (ORNL). Tristructural isotropic (TRISO)-coated particles and associated compacts for the AGR-5/6/7 experiment fabricated by BWX Technologies Nuclear Operations Group [Marshall 2020] were formed into a graphite matrix compact and irradiated at the Advanced Test Reactor at Idaho National Laboratory [Pham et al. 2021]. At ORNL, particles are deconsolidated from the graphite matrix compact and individually scanned for emitted gamma rays with the Irradiated Microsphere Gamma Analyzer (IMGA) [Baldwin et al. 2012, Hunn et al. 2013]. The IMGA system comprises a single high-purity germanium (HPGe) detector, an automated particle handling vacuum system, and an ORTEC DSPEC-50 digital spectrometer for gamma ray analysis. IMGA quantifies gamma ray-emitting fission product inventories of individual TRISO particles, and these inventories can be compared with the measured average inventories per particle and radionuclide inventories predicted by AGR-5/6/7 physics calculations [Sternbentz 2020] to determine if a particle experienced radionuclide release. Details on IMGA data collection methods can be found in the literature [Hunn et al. 2013].

The TRISO particle's SiC layer provides structural support, as well as a barrier for fission product release during irradiation or subsequent safety testing. A weakened or compromised SiC layer can be identified by the release of radionuclides, such as ^{137}Cs, which is detected by IMGA [Hunn et al. 2014]. However, select radionuclides, such as ^{90}Sr, ^{110m}Ag, and ^{154}Eu have been shown to migrate through an intact SiC layer [Hunn et al. 2013]. Measurement of the radionuclide ^{110m}Ag is significant as its release has been shown to be particularly sensitive to in-reactor conditions (e.g., temperature) with broad variable particle-to-particle release behaviors observed within a single compact. As such, ^{110m}Ag activity is often used for particle selection for comprehensive PIE as bounding ^{110m}Ag retention particles are hypothesized to represent limits in particle behaviors within a compact [Gerczak et al. 2018]. As TRISO particle fuel PIE activities continue over time, IMGA measurements of the ^{110m}Ag inventory are eventually hindered because of its relatively short half-life (~250 days). As the fuel ages from its end of irradiation (EOI) date, the measurement uncertainty and minimum detectable activity (MDA) of ^{110m}Ag increase because the detector background continuum begins to dominate. For particles from the second AGR irradiation experiment (AGR-2), the ^{110m}Ag MDA was above 20% of the calculated average particle inventory after approximately five half-lives, and ^{110m}Ag activity was no longer measurable with IMGA after approximately seven half-lives. Therefore, coincidence counting approaches have been explored to determine feasibility of leveraging new approaches to overcome limitations associated with increasing MDA over time.

1.1 COINCIDENCE COUNTING BACKGROUND

Coincidence counting is an active background-rejection technique in which an array of detectors is used in place of a single detector. Basically, if a gamma ray of interest is detected in one detector in the array, other gamma rays in the same decay cascade will likely be detected in another detector in the array within a small window of time (i.e., nanoseconds). This allows for rejection of time-random background and other undesired decays. Coincidence counting offers significant advantages for measuring precise absolute decay branching ratios or identifying and quantifying specific isotopes and materials, particularly in cases in which the radiation signature is weak when compared with other components of the spectrum or obscured by large background radiation.

An example of the coincidence technique is shown in Figure 1 with data from the CLARION Compton-suppressed HPGe detector array, which used to be located at the US Department of Energy Office of Nuclear Physics User Facility Holifield Radioactive Ion Beam Facility at ORNL [Allmond 2016].

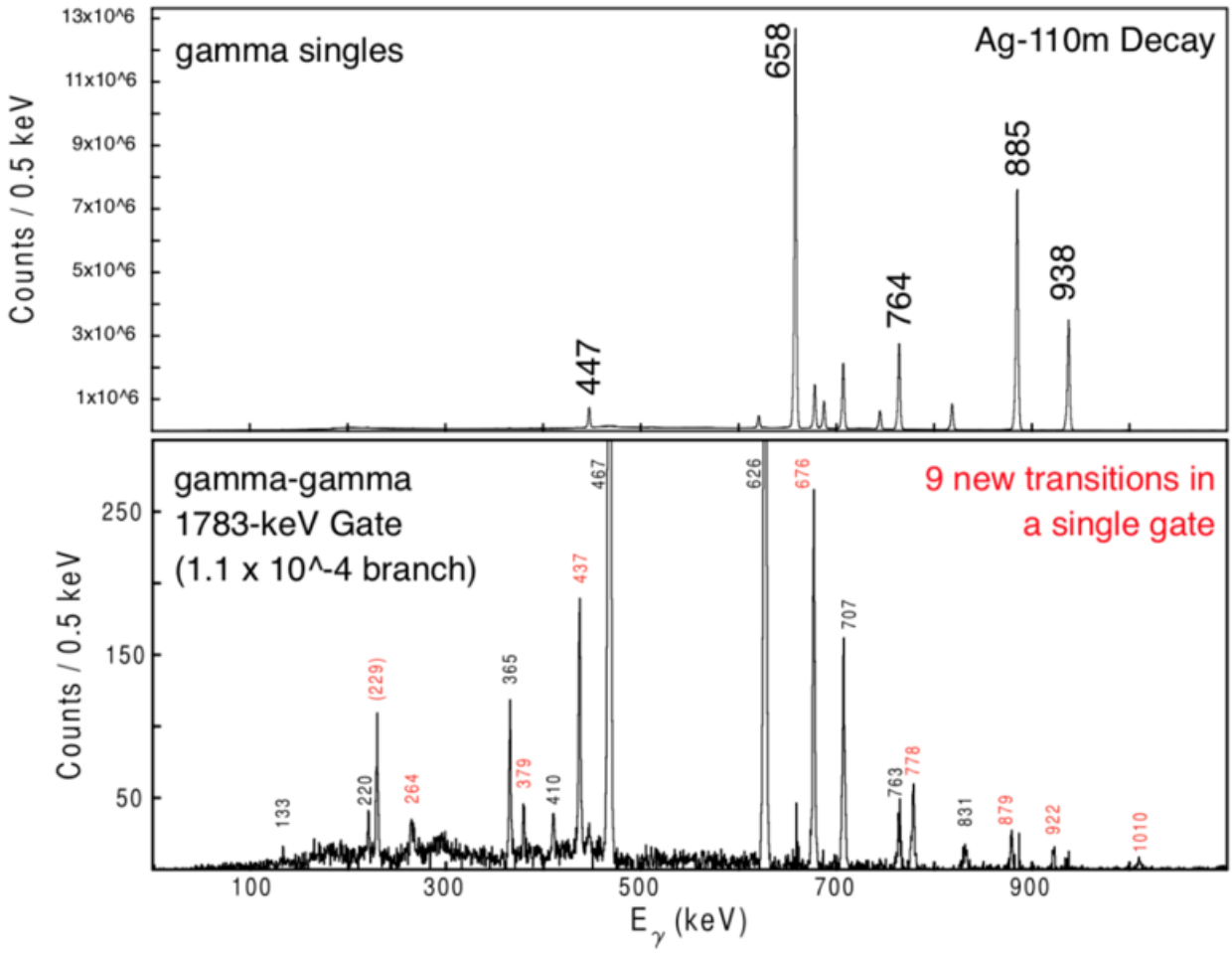

Figure 1. Two histograms showing a measurement with the CLARION detector of a silver foil that was irradiated within the High Flux Isotope Reactor [Gross et al. 2000]. (top) Measurement of radiation being emitted by the silver foil without any coincidences in place. The desired transition is not visible in this spectrum. (bottom) Spectrum using a coincidence gate placed on a 1783 keV gamma ray emitted by ^{110}Cd after ^{110m}Ag beta decay. This gate revealed nine previously unknown transitions in ^{110}Cd [Allmond 2016], demonstrating the selectivity of the technique and ability to suppress the background.

A thin, natural silver foil was irradiated at ORNL's High Flux Isotope Reactor [Gross et al. 2000] and subsequently counted. The top histogram in Figure 1 shows a traditional measurement of the radiation from the foil, usually referred to as a *singles* measurement. In this terminology, *singles* corresponds to what would be seen in a spectrum counting with a single HPGe detector. The bottom histogram shows coincidence data from ^{110}Cd following the beta decay of ^{110m}Ag that was extracted by looking for gamma rays in coincidence with a 1783 keV gamma ray (a previously known transition in ^{110}Cd). Many of the observed weak transitions (i.e., decay branches of 1 in 200,000 beta decays of ^{110m}Ag [Allmond 2016]) were otherwise inaccessible in the top histogram. Coincidence gates were set in software after collection.

This coincidence technique can be applied more generally to gamma-gamma, beta-gamma, alpha-gamma, fission-gamma, fission-beta-gamma, fission-beta-gamma-neutron, and more measurements to improve the signal-to-noise ratio and eliminate the need for background subtraction by counting room background levels for subtraction sample spectra. This improves MDA calculations because the background calculations performed for coincidence counting account for and allow for removal of the time-random

gamma-ray coincidences such as Compton scatter events. These events contribute heavily to the measured spectrum are not removable via traditional singles measurements.

The largest weakness of the coincidence counting technique is the increased measurement time required when compared with singles measurements. This effect can be countered by having more detectors and a consequentially larger and more expensive array. With an array of identical detectors, the total count time is dependent on the number of detector pairs (i.e., for N detectors, $N \times [N-1]$). This dependency means that doubling the number of detectors results in same number of counts in a coincidence spectrum in less than a quarter of the counting time. In more formal terms and without the assumption of an array of identical detectors, the total count time, t_{count}, is given by

$$t_{\text{count}} = \frac{N_{\text{count}}}{I_\gamma R_{\text{o}}} \sum_{i,j,i\neq j} \frac{1}{\varepsilon_i \varepsilon_j}, \tag{1}$$

where N_{count} is the desired number of counts in coincidence, R_{o} is the activity of the source for a given coincidence in counts per second, I_γ is the absolute branching ratio of the gamma ray of interest, ε_i is the efficiency of the i^{th} detector in the array, and ε_j is its detector pair. Count time can also be shortened by more efficient detectors and/or detectors that may stand closer to the array (without collimation), thus covering more solid angle.

1.2 CHOOSING CANDIDATES FOR COINCIDENCE MEASUREMENTS

The coincidence technique is only applicable for nuclei that emit particles in coincidence, whether that is a beta particle and a gamma ray, two or more gamma rays, an alpha particle and a gamma ray, or other combinations. In the case of $^{110\text{m}}$Ag, an examination of the known decay schemes yield optimal signature transitions for the coincidence method. In this study, only gamma-gamma coincidences were considered.

Decay schemes of $^{110\text{m}}$Ag provided online by the National Nuclear Data Center (NNDC) in the Evaluated Nuclear Structure Data File (ENSDF) were examined. Coincidences between gamma rays at 1384.3 keV (24.8%), 884.7 keV (74.6%), and 657.8 keV (100%) were considered first. These gamma rays represent a cascade between levels at 2926.7 keV to 1542.4 keV to 657.8 keV to the ground state. Coincidences between gamma rays at 763.9 keV (22.9%), 1505.0 keV (13.3%), and 657.8 keV (100%) were also considered, which form a cascade from the level at 2926.7 keV to 2162.8 keV to 657.8 keV to the ground state. These cascades are of particular interest because the gating gamma rays at 1384.3 keV and 1505.0 keV are strongly produced and will be above the Compton continuum, as well as the region crowded by peaks from other fission products. Therefore, these cascades are likely to produce a clean gated spectrum, though 884.7 keV might still be used. One other cascade was explored, namely the cascade of 937.5 keV (35.4%), 884.7 keV (74.6%), and 657.8 keV (100%) of gamma rays de-exciting the levels at 2479.9 keV to 1542.4 keV to 657.8 keV to the ground state. This cascade is of interest because of its strength.

1.3 ARRAY TYPES

The first, most obvious option to implement coincidence counting for TRISO fuel PIE is to simply expand the number HPGe detectors from one to an array. The exact number of detectors required depends on the desired count time per particle. When designing any coincidence counting array, time-random events between detectors must be minimized so that the available detector count rate is not occupied, leaving a maximum of dynamic range for desired coincident events. This minimization is achieved through optimizing the detector distance from the source such that pulses do not pile up inside a single given detector, increasing detector dead time. If the detector is not overwhelmed, this background may be subtracted. Time-correlated background events may not be subtracted; however, to minimize these events,

the detectors in an array should not be placed directly across from one another to minimize simultaneous 511 keV annihilation gamma-ray events. Similarly, placing shielding between detectors will minimize Compton scatter events between detectors. The disadvantage of shielding is that it will provide its own opportunities for Compton scatter. The further downsides of an HPGe-only array include an increased need for floor space to accommodate the cooling systems and increased array complexity, although commercial options exist to address these issues.

A second highly viable option is a mixed array of HPGe and another detector type, preferably one that has higher efficiency and can sustain higher count rates. This mixed array could be placed closer to the radioactive source, resulting in significantly reduced count times. Lanthanum bromide is an excellent option that has been demonstrated in high-rate environments [Drescher et al. 2017]. Lanthanum bromide is a highly efficient inorganic scintillator and requires no cooling. It has a 16–24 ns decay time vs. 6 μs for HPGe. Lanthanum bromide can count at 25 times the rate of an HPGe and may consequently be placed closer to the radioactive source [Luxium Solutions 2023]. The downside of LaBr is its significantly worse energy resolution when compared with HPGe. The resolution of LaBr is 2.2% of the full width at half maximum at 662 keV (^{137}Cs) compared to 0.2% for an HPGe; a spectrum for a 3-inch (7.62 cm) LaBr detector is shown in Figure 2.

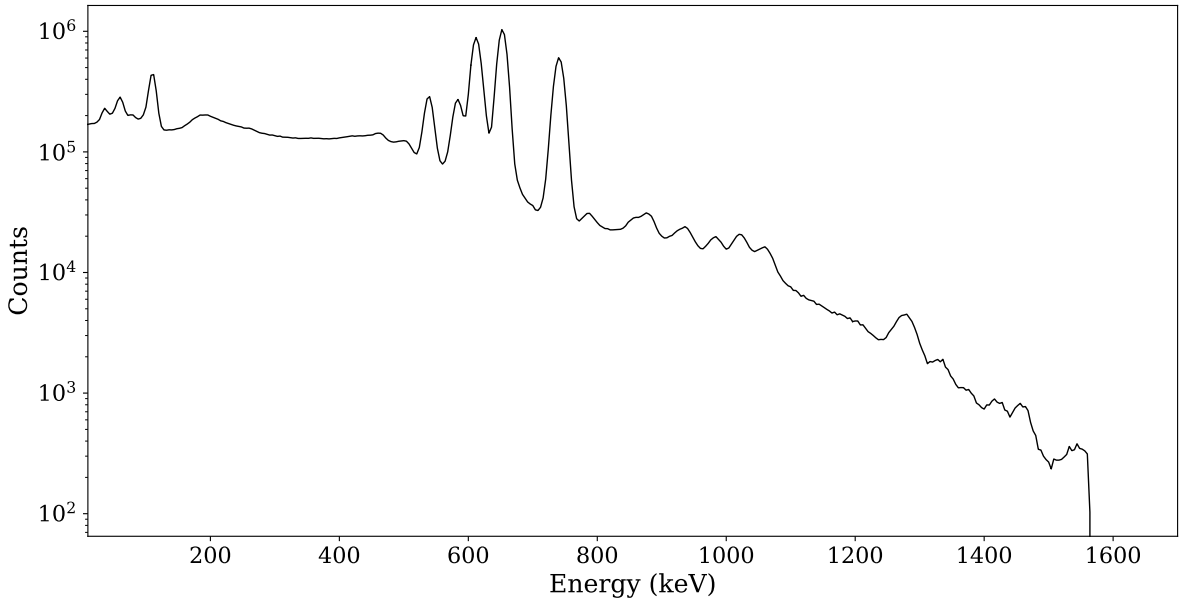

Figure 2. Three-inch (7.62 cm) diameter LaBr spectrum of TRISO fuel (AGR-5/6/7 Particle 221-RS24).

The reduction in resolution means that in a mixed array, the HPGe detectors should be used as the gating detectors, and the LaBr detectors should only be used to generate the coincidence spectra after the gate as that is a significantly less crowded spectrum. An example of a mixed array is shown in Figure 3 on the bottom. The final array possibility, which is likely beyond the needs of this program but is mentioned for completeness, is the inclusion of bismuth germanium oxide (BGO, a.k.a. bismuth germanate) shielding for Compton suppression. BGO is a heavy inorganic scintillator like LaBr but with a 10× worse resolution than LaBr. Because BGO is very high Z and dense, it is useful as an anticoincidence for rejecting Compton events between detectors, thus significantly reducing time-random background events. An example of an array of HPGe detectors with BGO shielding is shown in Figure 3 on the top.

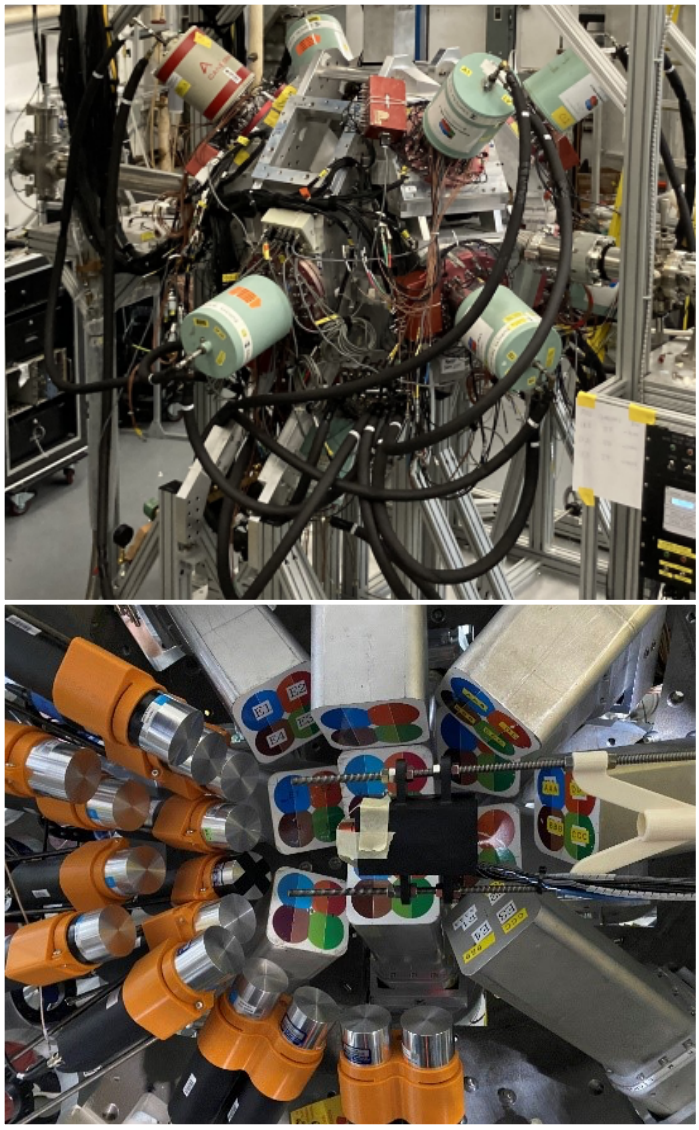

Figure 3. Recent large HPGe arrays built and led by ORNL. (top) CLARION2-TRINITY at the John D. Fox Laboratory at Florida State University [Gray et al. 2022], and (bottom) interior view of The Facility for Rare Isotope Beams (FRIB) Decay Station initiator (FDSi) [FDSi Coordination Committee 2020] composed of clover (four per detector) HPGe detectors and two-inch (5.08 cm) LaBr detectors.

2. EXPERIMENT METHODS

The objectives of this experiment were to

- measure an AGR-5 TRISO particle with the prescribed coincidence counting method (given in Section 2.2) that had a previously IMGA-measured ^{110m}Ag inventory;
- compare ^{110m}Ag activity, measurement uncertainty, and MDA calculated from coincidence counting to those of IMGA;
- calculate the number of detectors and acquisition time needed for coincidence counting measurements to be successful for AGR PIE; and
- recommend future work to either further coincidence counting analysis or decide on the feasibility of coincidence counting for AGR PIE.

2.1 MATERIAL

AGR-5/6/7 Compact 2-2-1 was deconsolidated to recover individual particles for IMGA examination. Irradiation conditions of Compact 2-2-1 are given in Table 1. Further information on the deconsolidation and particle recovery process can be found in the literature [Hunn et al. 2013; Baldwin et al. 2012]. After IMGA initially scanned 2237 Compact 2-2-1 particles, a random subset of 63 particles was riffled from the 2237, and each particle was scanned at a longer acquisition time of 4 h to measure lower-activity radionuclides, such as ^{110m}Ag. Particle 221-RS24 was selected for coincidence counting, and its ^{110m}Ag inventory data are given in Table 2.

Table 1. Irradiation conditions for AGR-5/6/7 Compact 2-2-1

Compact ID [a]	Number of particles examined by IMGA	Average burnup [b] (FIMA, %)	Fast fluence [b] ($E > 0.18$ MeV, neutrons/m^2)	TAVA temperature [c] (°C)
AGR-5/6/7 2-2-1	2237	14.03	4.72×10^{25}	845

[a] The X-Y-Z compact identification (ID) convention denotes the location in the irradiation test train: Capsule-Level-Stack.
[b] Burnup in fissions per initial metal atom (FIMA) [Sterbentz 2020, Table 9] and fast fluence [Sterbentz 2020, Table 12] are based on physics calculations.
[c] Time-averaged, volume-averaged (TAVA) temperature is based on thermal calculations [Hawkes 2021].

Table 2. AGR-5/6/7 Particle 221-RS24 ^{110m}Ag measured inventory data from IMGA

Particle ID	Measured ^{110m}Ag inventory [a] (Bq)	Measurement uncertainty (%)	MDA [a] (Bq)	MDA/calculated ^{110m}Ag (%)
221-RS24	3.642×10^4	18.0	1.265×10^4	11.9

[a] Activity is decay corrected to EOI +1 day date, July 23, 2020, 03:10:00 EST.

2.2 EXPERIMENTAL SETUP

The experimental plan involved setting up an array of three HPGe detectors and collecting data from a single particle of TRISO fuel with a multichannel digital acquisition system, as shown in Figure 4. The digitizer was required for time correlation across detectors in the array. Data were collected for a period of days to weeks, after which the data were processed and examined for coincidences, as outlined in Section 1.2.

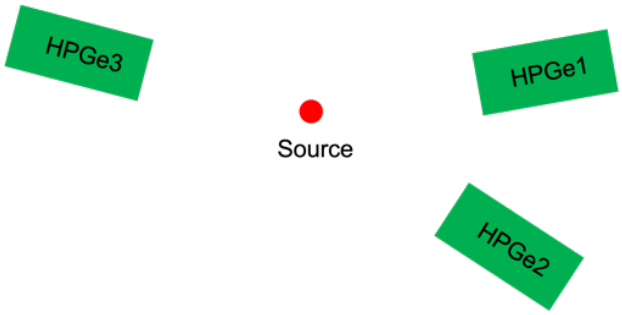

Figure 4. Top-down view showing the array geometry of the initial setup with three HPGe detectors.

HPGe1 and HPGe2 were ORTEC pop-top HPGe detectors of model numbers GMX15P4-70-ST and GMX-45200-P, respectively, cooled by floor-standing dewars with a liquid nitrogen autofill system attached. The third HPGe detector, HPGe3, was a Canberra mechanically cooled HPGe detector with model number GC1018 with cryostat model CP5-PLUS-F-RDC-4. All three detectors were powered with ORTEC 556 high-voltage power supplies located in a nuclear instrument module crate about a meter away from the setup. Data were collected using a Pixie16 16-channel digitizer from XIA LLC located in the same crate with acquisition and analysis codes developed at ORNL in C and C++, respectively. Optical detector distances were determined by pulling each HPGe back from the source until a sustained count rate of approximately 15 kHz was measured on the digitizer; this measurement is the maximum before detector pileup and dead time become a concern. Unfortunately, after only a couple days of counting with this setup, a power outage rendered HPGe3 nonfunctional. The cause of the failure is believed to be because of quick bias cycling on the detector and perhaps some detector warming, as that was the mechanically cooled detector. Researchers are unsure of the duration of the outage.

Counting proceeded for two weeks using only HPGe1 and HPGe2, yielding some good initial results discussed in the following sections. At this point, more detectors were determined to be required for the array to count in a reasonable amount of time, so three LaBr crystals were borrowed from the University of Tennessee, Knoxville and were arranged in the geometry shown in Figure 5.

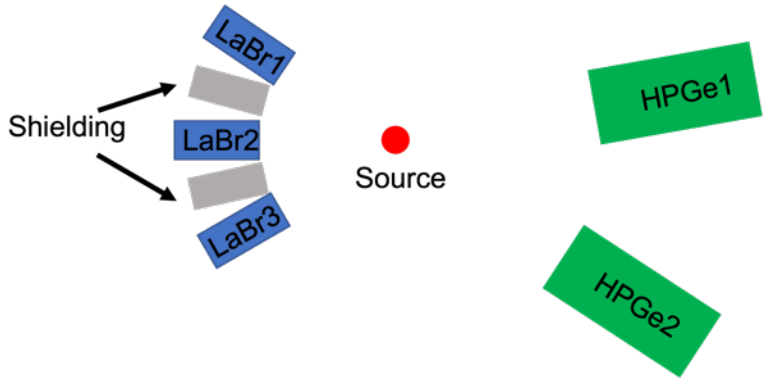

Figure 5. Top-down view showing the geometry of the follow-on setup with two HPGe detectors and three LaBr detectors, with shielding between the detectors. The shielding's purpose is to minimize time-coincident Compton scatter events between the detectors.

The detectors and the crate holding the high-voltage power supplies were plugged into an uninterruptible power supply to provide a buffer against future possible power failures. This second setup with the added capability of the additional LaBr detectors was run continuously for two months, yielding a large amount of data for analysis. That analysis, which is computer intensive due to the amount of available data, is ongoing and will be reported in a later publication.

2.3 DATA ANALYSIS

Before any coincidence spectra could be built, the first step in the data analysis was to calibrate the singles spectra. As introduced in Section 1.1 and for the purposes of the following discussion, *singles* refers to the spectrum from a single detector, and *coincidence* refers to the spectrum from the array, either in whole or in part. Because irradiated TRISO fuel is well-characterized and emits abundant gamma rays, the peaks present in the spectrum from the sample particle were used for energy calibration. The gamma rays chosen for calibration are shown in Table 3.

Table 3. Lines present in spectrum that were used to calibrate

Nucleus	Energy (keV) [a]	HPGe	LaBr
^{144}Ce	133.515	X	X
^{106}Rh	511.861	X	X
^{134}Cs	604.721	X	X
^{137}Cs	661.657	X	X
^{134}Cs	795.864	X	X
^{154}Eu	1274.429	X	—

Note: X marks that a given gamma ray was used for that detector type.
[a] Gamma peak energies from ENSDF [National Nuclear Data Center].

After identifying the appropriate peaks in the spectrum, a first-order linear curve was fit to the data to extract the calibration coefficients. The resulting calibration is shown in Figure 6 for the HPGe detectors, and the calibrated spectra for both are shown in Figure 7. The spectra of the two HPGe detectors are not identical because the detectors, one of which was borrowed, are not the same volume and have different preamplifiers and associated hardware.

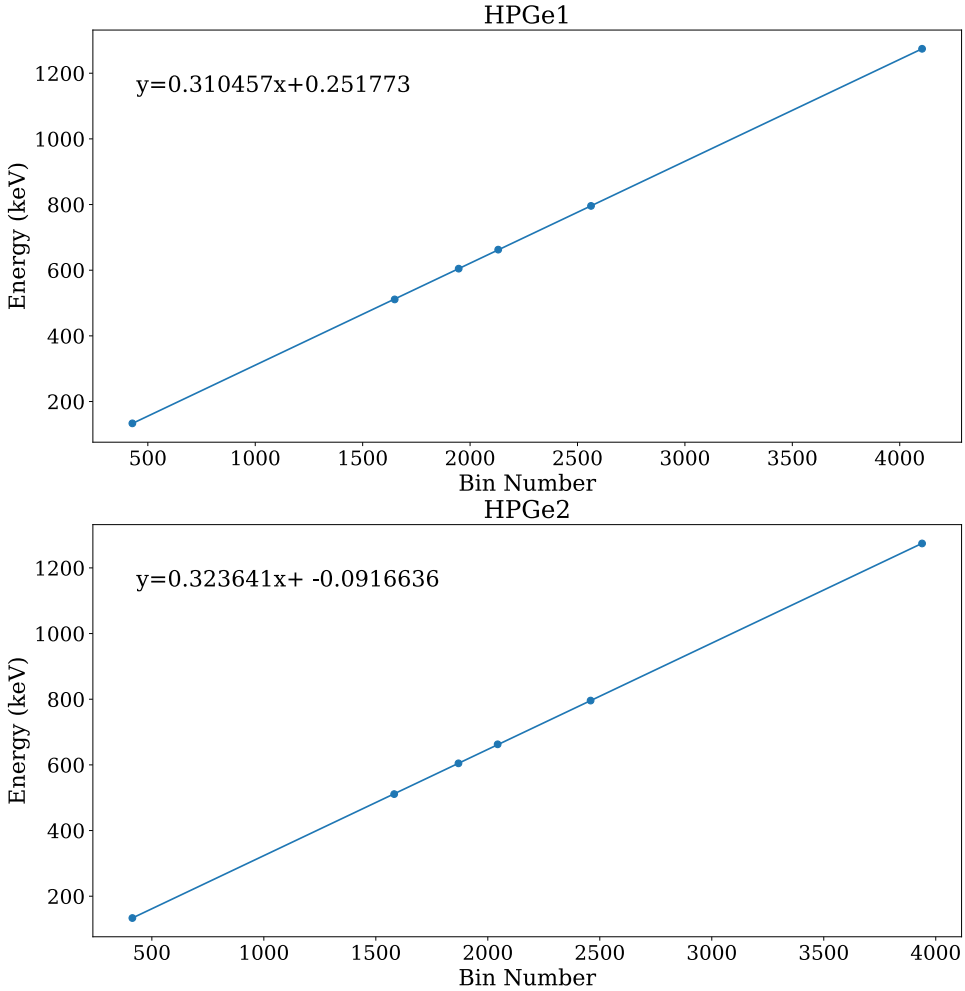

Figure 6. Plots showing the results of the linear fit and extracted energy calibration coefficients for both HPGe detectors.

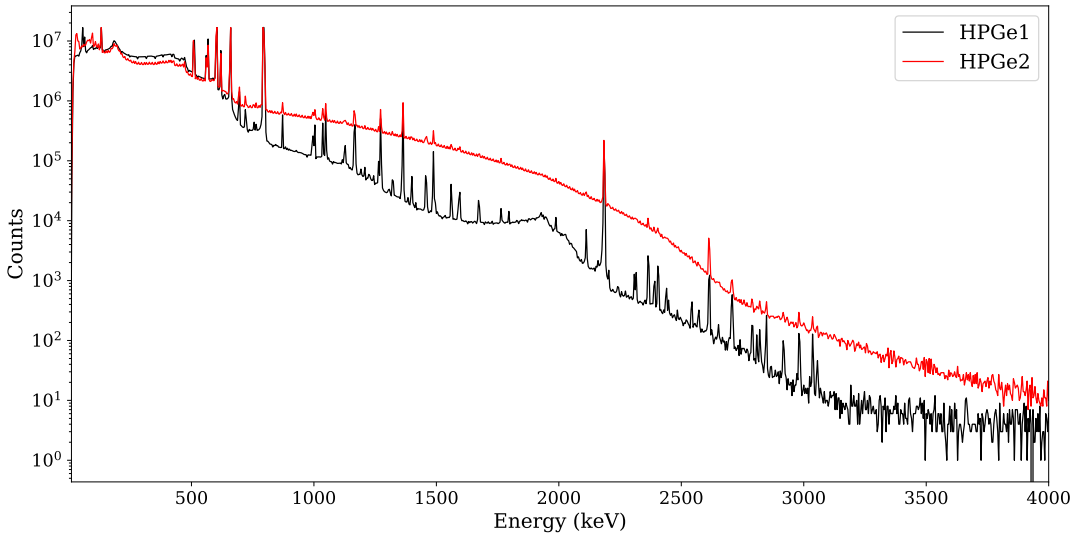

Figure 7. Calibrated singles spectra for both HPGe detectors.

The second step of the data analysis was to find the appropriate event window to build the coincidence spectra. This is a critical step of the analysis because if the window is too wide, an excess of time-random coincidence events will produce unnecessary background, and if the window is too small, valid events will be excluded from the analysis. To judge the correct window, the time different between the one detector to trigger in a given event window and the second detector pre- and post-trigger were plotted vs. time in nanoseconds pre- and post-trigger; the result is shown in Figure 8.

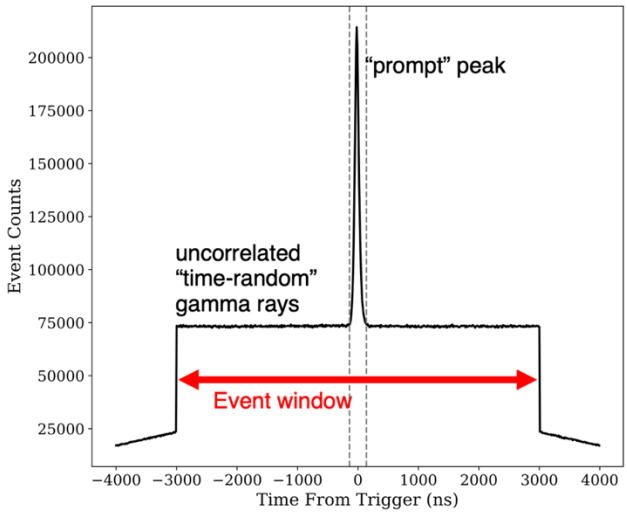

Figure 8. Coincidence window selection plot for the HPGe detectors. The dotted lines mark the appropriate coincidence window for this detector.

The height of the square wave in Figure 8 shows the number of time-random coincidences during the larger event window (±3000 ns). The peak in the center is referred to as the *prompt* peak and represents correlated events (multiple gamma-rays that are emitted from a single nuclear decay) plus a background of time-random events (uncorrelated gamma-rays that happen to be emitted within ~300 ns of each other). The appropriate coincidence window to best exclude time-random background events is shown with the dotted lines. In this study, for the HPGe detectors only, events built into the coincidence spectra were

from +140 ns after the trigger and −140 ns pretrigger. The event window plots provide a further insight into the utility of a possible mixed array. The number of counts vs. time for the event window for each iteration of the array is shown in Figure 9. Lanthanum bromide produced nearly an order of magnitude more counts during the desired event window than that of HPGe alone, indicating a similarly reduced count time.

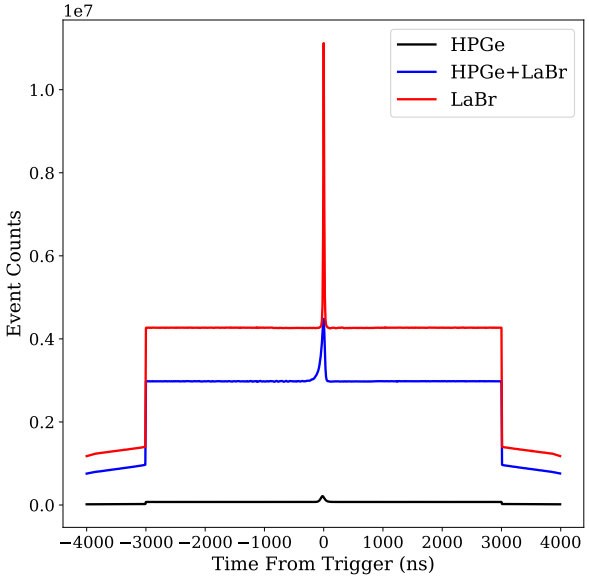

Figure 9. Event window plot for (black) the HPGe detectors only, (blue) a mix of HPGe and LaBr detectors, and (red) LaBr detectors only.

Furthermore, because LaBr has better time resolution than HPGe, a tighter prompt window can be used reducing the time-random event contribution to spectra. This increases the signal-to-noise ratio and reduces statistical fluctuations in the final background-subtracted spectra. A comparison of the normalized HPGe prompt peaks and LaBr prompt peaks is shown in Figure 10.

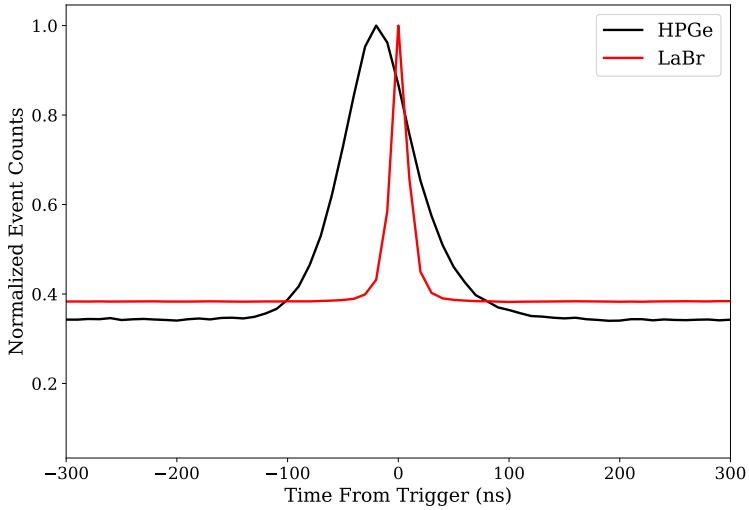

Figure 10. Prompt peaks in the event window for HPGe and LaBr detectors. The event counts are normalized to unity to provide a proper comparison. The LaBr coincident event window is an order of magnitude shorter than the HPGe coincident event window.

With the selection of a proper coincidence event window, coincidence spectra could be made. These spectra were achieved through selecting events in which two detectors triggered during the larger event window (±3000 ns). Events were then further down-selected so that only events occurring during the much smaller (±140 ns) "prompt" coincidence event window were kept. In the case of HPGe detectors, the spectrum of one HPGe to trigger during the event window was plotted on the *y*-axis, with the second HPGe on the *x*-axis, resulting in a 2D histogram such as that shown in Figure 11.

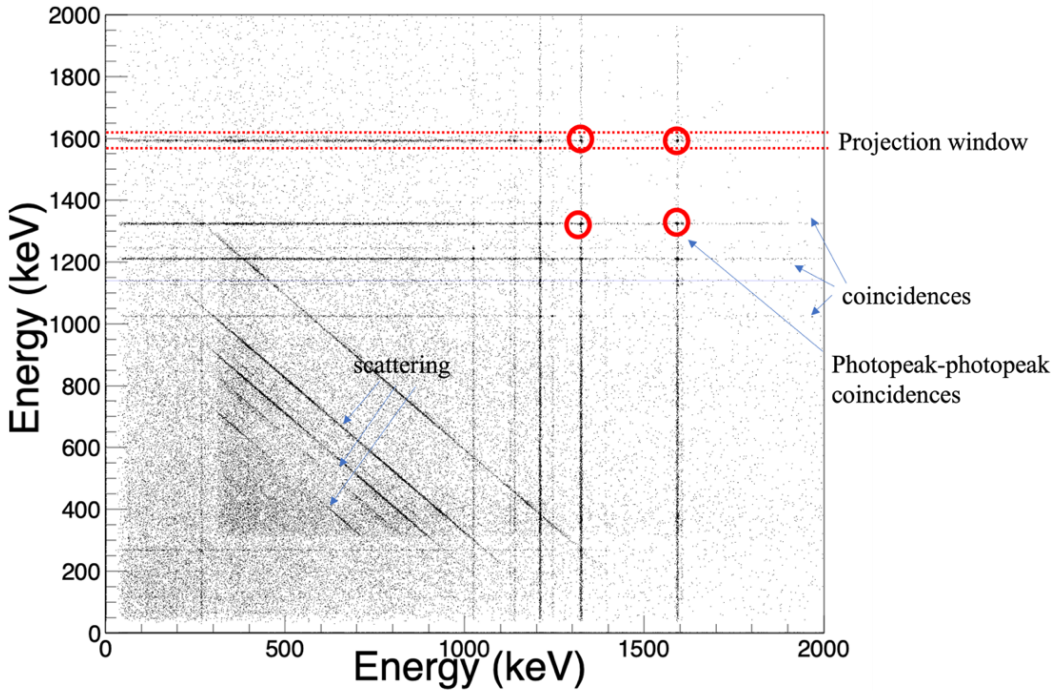

Figure 11. Important features in a gamma-gamma coincidence spectrum. The horizontal and vertical lines are coincidences, the red dashed line shows an appropriate projection window to look for coincidences around 800 keV (0.5 keV/channel), and the diagonal lines are time-coincident events that occur in both detectors, mostly Compton scatter.

The vertical and horizontal lines in the gamma-gamma coincidence spectrum, highlighted in Figure 11, represent coincidence events between a photopeak in one detector, and a Compton scatter in the second detector (although some will be time-random given the high activity of the sample). The peaks highlighted with small circles indicate photopeak-photopeak coincidences. The diagonal lines represent scattering events across the two detectors. Background subtraction is performed through selecting event data on the positive and negative sides of the trigger in the event window plot. When plotted together, these form background coincidence spectra. Those spectra are then scaled and subtracted from the coincidence spectrum, leaving a clean spectrum from which to proceed. In the case of the HPGe detectors, background data were chosen between +660 – +1660 ns and -1660 – -660 ns, as shown in Figure 12.

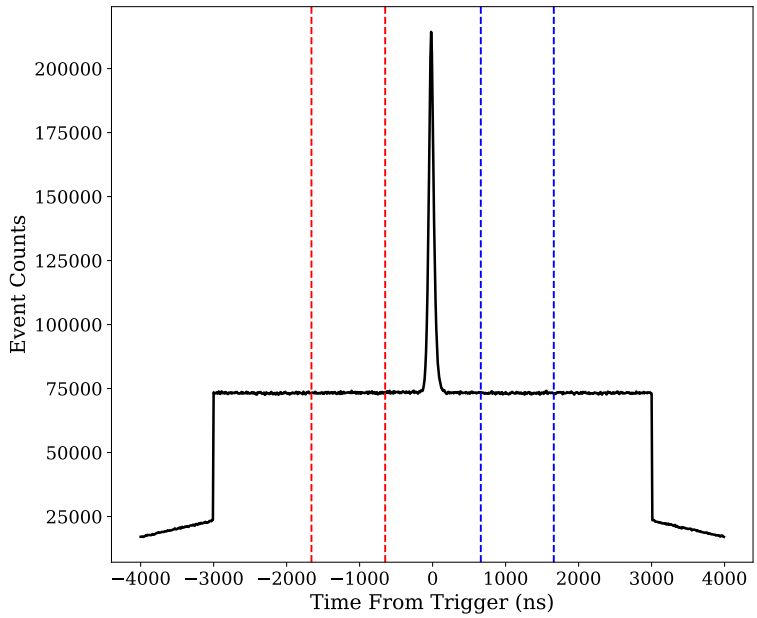

Figure 12. Event window selection plot for the HPGe detectors. The dotted lines mark the appropriate event window for use in background subtraction in the detector.

To extract a final coincidence spectrum, a gate was placed around a single horizontal line in the coincidence spectrum and then projected onto the *x*-axis. In this way, the *y*-axis was used as an energy gate. An example of the final spectrum is shown in Figure 13. In this study, to look for coincidences at 657.8 keV, a projection was taken between 656 and 659 keV on the *y*-axis. If a projection onto the *x*-axis were taken across the entire *y*-axis, the singles spectrum would be recovered.

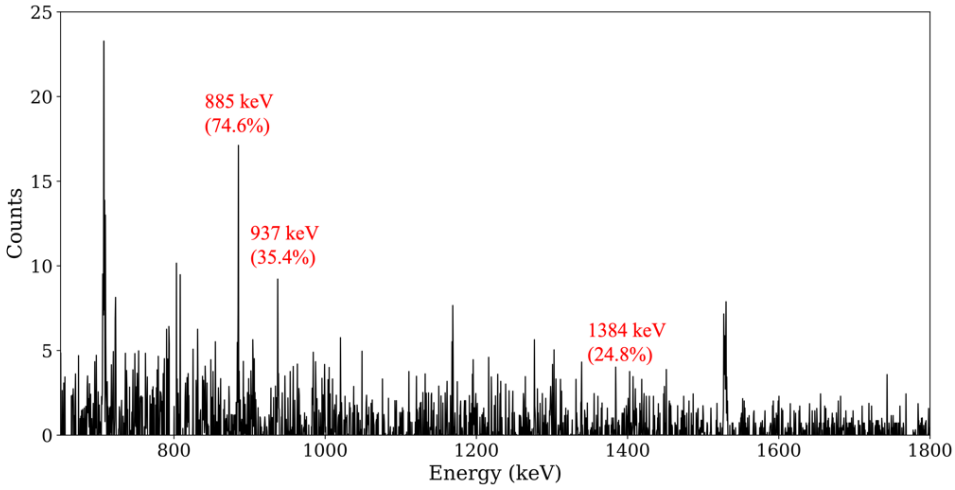

Figure 13. Final coincidence spectrum on a subset of data. This graph is a coincidence spectrum using 657.8 keV as a gate by taking a projection between 656 and 659 keV on the *y*-axis down onto the *x*-axis from the data in Figure 11. Three coincident gamma rays with their absolute gamma intensity per ENSDF [National Nuclear Data Center] are highlighted in red.

A similar technique was deployed for examining coincidences that included LaBr, except the HPGe detector was always on the *y*-axis, and the *x*-axis was based on input from both LaBr and HPGe detectors.

This technique resulted in the HPGe data being used as a gate and the final coincidence spectrum being composed of the less well-resolved but much less crowded LaBr + HPGe spectra.

The final calculation of activity from the coincidence spectrum is very similar to the traditional method of calculating activity from a singles spectrum. The gamma ray of interest in the spectrum shown in Figure 13 is fit with a Gaussian curve on a linear background to calculate the total area under the peak. The activity R of the desired isotope is given most generally by Equation 2:

$$R = \frac{N}{E_{\text{double}} I_\gamma t}, \tag{2}$$

in which N is the number of counts in the peak minus any background, t is the count time in seconds, and I_γ is the absolute branching ratio of the gamma ray, obtainable from any nuclear database. E_{double} is the absolute doubles efficiency of the system given by:

$$E_{\text{double}} = \sum_{i,j,i\neq j} E_i E_j \,, \tag{3}$$

in which E_i is the absolute efficiency of each detector in the array. Generally, E_i is given by:

$$E_{i,j} = \frac{\varepsilon_{i,j}\Omega_{i,j}}{4\Pi}, \tag{4}$$

in which $\varepsilon_{i,j}$ is the efficiency the i^{th} or j^{th} detector in the array and $\Omega_{i,j}$ is its solid angle. For a cylindrical detector this becomes:

$$E_{i,j} = \frac{\varepsilon_{i,j} r_{i,j}^2}{4 d_{i,j}}, \tag{5}$$

in which $r_{i,j}$ is the radius of the detector and $d_{i,j}$ is the distance of the detector from the source.

Alternatively, with a coincidence counting setup the total efficiency E_{double} of the system may be experimentally and more exactly measured through taking a coincidence spectrum on a ^{60}Co source or with the sample itself, if there are enough strong coincident gamma rays from the sample. To use ^{60}Co as an example, because the two gamma rays from ^{60}Co at 1173.2 keV and 1332.5 keV always occur in coincidence, the efficiency of each detector can be measured by taking the ratio of the number of 1173-1332 coincident counts, N_{gg}, to the number of counts in the same peak in the singles spectrum N_{single}: $\frac{N_{gg}}{N_{single}}$. Thus, for a two-detector array:

$$E_{\gamma 1} = \frac{N_{gg}(\gamma_2, \gamma_1)}{N_2(\gamma_2)}, \tag{6}$$

$$E_{\gamma 2} = \frac{N_{gg}(\gamma_1, \gamma_2)}{N_2(\gamma_1)}, \tag{7}$$

in which $N_{gg}(\gamma_2, \gamma_1)$ denotes the number of times the 1173-keV gamma ray is detected in detector 1 and the 1332-keV gamma ray is detected in detector 2, and $N_2(\gamma_2)$ indicates the number of counts in the 1332 keV peak in the singles spectrum from detector 2.

The most exact method is to use gamma rays from the radioactive sample itself as there are no slight changes to geometry, i.e., source placement, that could contribute to systematic error in the efficiency correction curve. Because ^{134}Cs decay is strongly represented in the AGR TRISO gamma ray spectrum, the 795.9 and 604.7 keV coincident gamma rays were used to generate an absolute gamma ray efficiency measurement at two gamma ray energies. A relative gamma ray efficiency curve was then generated with 563.2, 569.3, 604.7, 795.9, 802.0, 1168.0, and 1365.2 keV peaks. This relative efficiency measurement was scaled with the absolute efficiency and fit with a third order polynomial to provide an energy-dependent efficiency correction for the absolute activity measurements. Because the gamma rays used for the absolute efficiency measurement are part of a $4^+ \rightarrow 2^+ \rightarrow 0^+$ cascade and are therefore emitted anisotropically, an angular correction, ε_θ, was applied [Morrison 2015; Lauritsen et al. 2016]. ε_θ is given by

$$\varepsilon_\theta = \frac{1.05}{W(\theta_{\gamma\gamma})/W(90)}, \tag{8}$$

in which $\theta_{\gamma\gamma}$ is the measured angle between a detector pair, in this case 15°, and

$$\frac{W(\theta_{\gamma\gamma})}{W(90)} = 1 + \frac{1}{8}\cos^2(\theta_{\gamma\gamma}) + \frac{1}{24}\cos^4(\theta_{\gamma\gamma}). \tag{9}$$

The final correction was a 0.82 pileup correction factor indicating that 0.28% of all events in the detectors were pileup events as measured by the Pixie16 digitizer.

3. RESULTS

Figure 14 illustrates particle 221-RS24's IMGA-acquired gamma-ray spectrum centered on the 884.7 keV ^{110m}Ag photopeak of interest in comparison to the 873.2 keV peak from ^{154}Eu. The total area of the ^{110m}Ag photopeak, which is used to calculate activity, was approximately 6% of the detector's background area counts (continuum), which contributed to the measurement uncertainty and MDA.

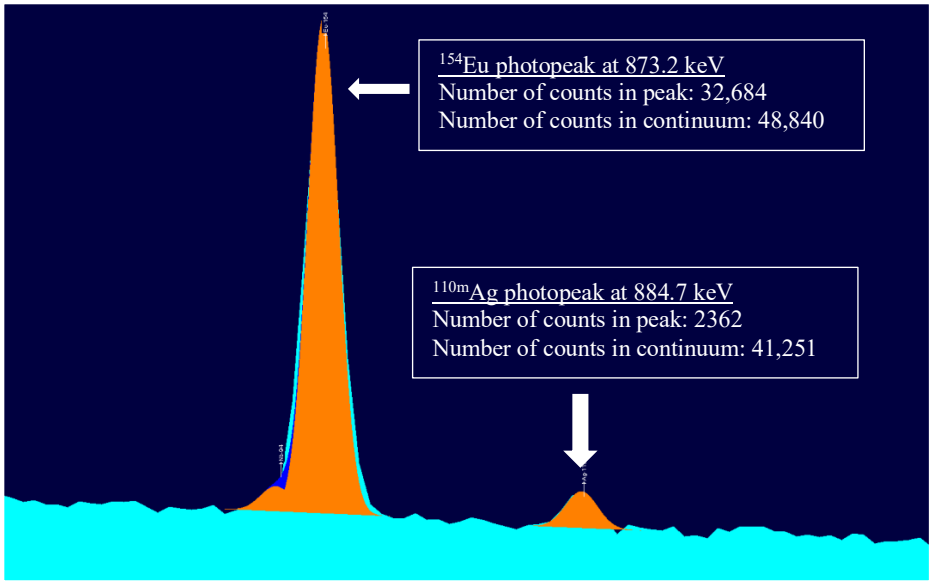

Figure 14. IMGA spectrum focused on ^{110m}Ag photopeak at 884.7 keV.

Data was analyzed from nineteen days of counting with two HPGe detectors. The gamma ray at 657.8 keV is produced in 100% of ^{110m}Ag beta decays as it is the gamma ray de-exciting the first excited state to the ground state of ^{110}Cd whereas the 884.7 keV gamma ray only occurs 74.6% of the time [National Nuclear Data Center, ENSDF]. The stronger 657.8 keV gamma ray is not commonly used in MDA analysis of ^{110m}Ag however because in singles spectra it forms a doublet with the much stronger 661.7 keV gamma ray from the beta decay of ^{137}Cs and is therefore indistinguishable. However, during the analysis it was discovered that gating on 884.7 keV yielded a clear 657.8 keV peak in coincidence spectra, as shown in Figure 15. This peak is clear enough in the data to be used to calculate ^{110m}Ag activity.

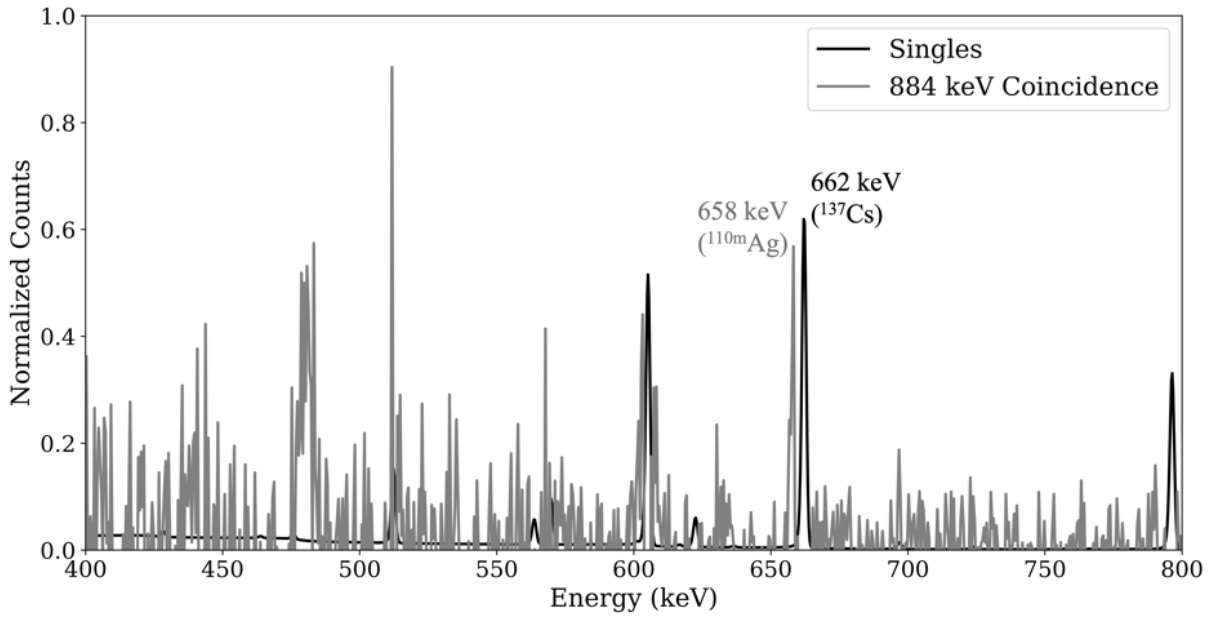

Figure 15. Normalized spectra of singles (black) and coincidence gated on 884.7 keV (gray) demonstrating a clear peak at 657.8 keV.

Furthermore, it provided clear and visible bounds on which to apply a second gate, this time on 657.8 keV. This gate is, no doubt, contaminated with a large 661.7 keV contribution, however for our purposes this does not cause any issues as the only member of the 661.7 keV cascade in ^{137}Cs is a 32 keV x-ray, well below the range of gamma rays that are pertinent for coincidence measurements in ^{110m}Ag. Therefore, the energy range of the 657.8 keV gamma ray derived from the coincidence spectrum gated on 884.7 keV was used to provide a 657.8 keV gated coincidence spectrum, as shown in Figure 16. The coincidence spectrum (bottom) shows an essentially *background-less* spectrum with ^{110m}Ag gamma rays 884, 937, and 1,384 keV clearly visible. The comparison to the singles spectrum (top) is to demonstrate that these peaks are difficult to fully resolve with a standard singles measurement and certainly subject to large amounts of background and interference from other gamma rays. The coincidence spectrum allows for very precise measurements of ^{110m}Ag content given an appropriate counting period because no Compton background or competing gamma rays exist to subtract from the calculation of the number of counts in the peak.

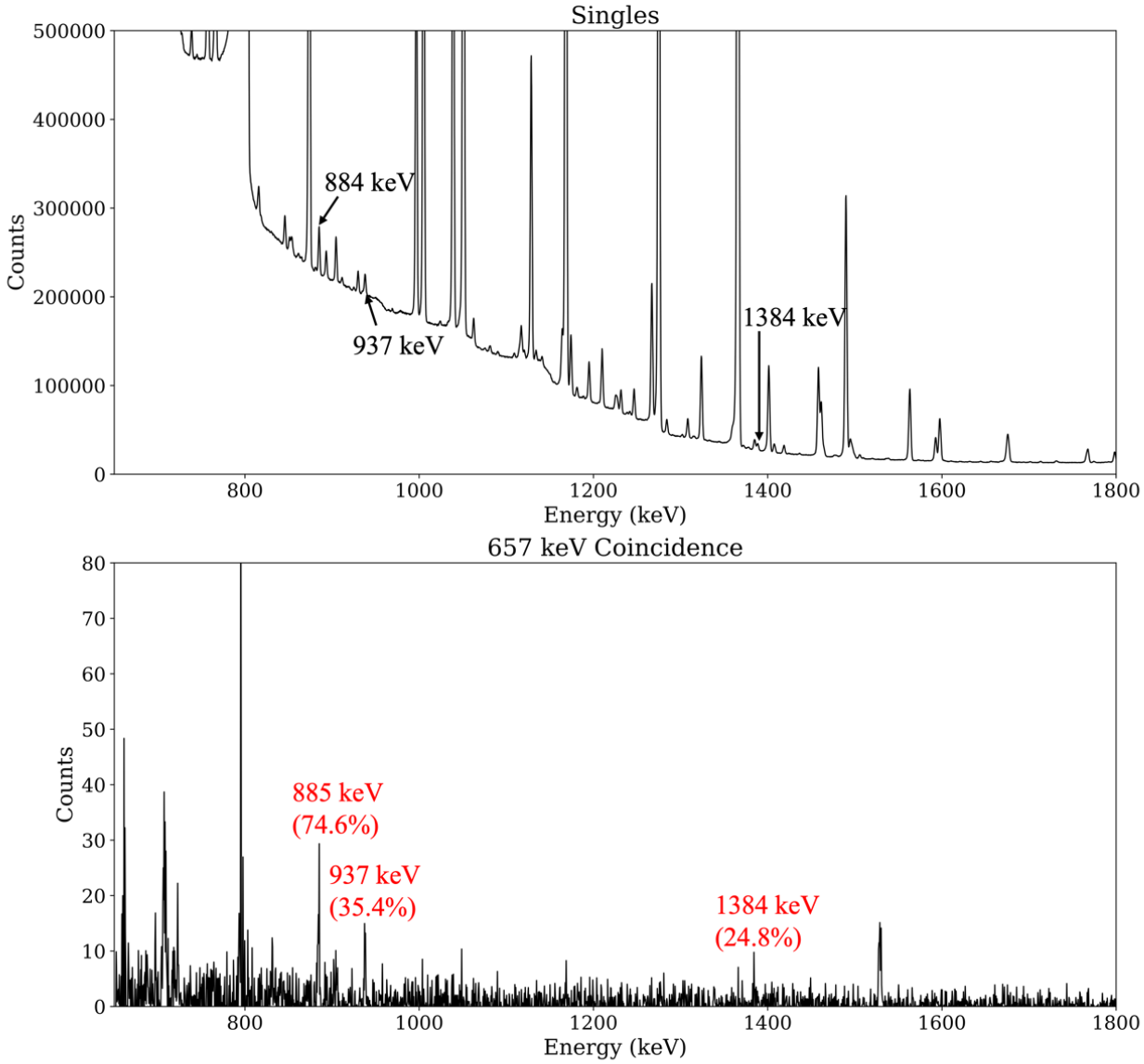

Figure 16. Coincidence results for (bottom) 884.7 keV compared with (top) original singles spectrum.

The peaks in the coincidence spectra were summed to provide a peak area or N in Equation 2. Errors were calculated as the summation in quadrature of the error associated with the fit, the error in the gamma ray data from the NNDC and an arbitrarily assumed 5% error to account for other systematic effects.

The total activity and the associated error were calculated using Equation 2 with the E_{double} calculated using the method described in the Section 2.3. The activities were then backdated to one day after the EOI (July 23rd, 2020 3:10 EST) as per standard operating procedure yielding the final results displayed in Table 4 and Figure 17.

Table 4. Activities (Bq) for particle 221-RS24 decay-corrected to one day after the EOI.

Energy	"Singles" [a]	"Coincidence" [b]	3σ Detection Limit [c]	IMGA [d]	MDA
884.7 keV	$3.5(2) \times 10^4$	$3.8(5) \times 10^4$	2.1×10^3	$3.2(6) \times 10^4$	$1.1(10) \times 10^4$
937.5 keV	$3.7(2) \times 10^4$	$3.6(10) \times 10^4$	4.6×10^3	—	—
1384.3 keV	$4.3(3) \times 10^4$	—	5.3×10^3	—	—
1505.0 keV	$3.8(4) \times 10^4$	—	2.9×10^3	—	—

Note: parentheses denote uncertainty in reported value.
[a] Efficiency determined in situ through gamma-gamma coincidence following ^{134}Cs decay.
[b] The coincidence gate was placed on 657.8 keV.
[c] Detection limit in singles based on local background fluctuation.
[d] Efficiency determined from source.

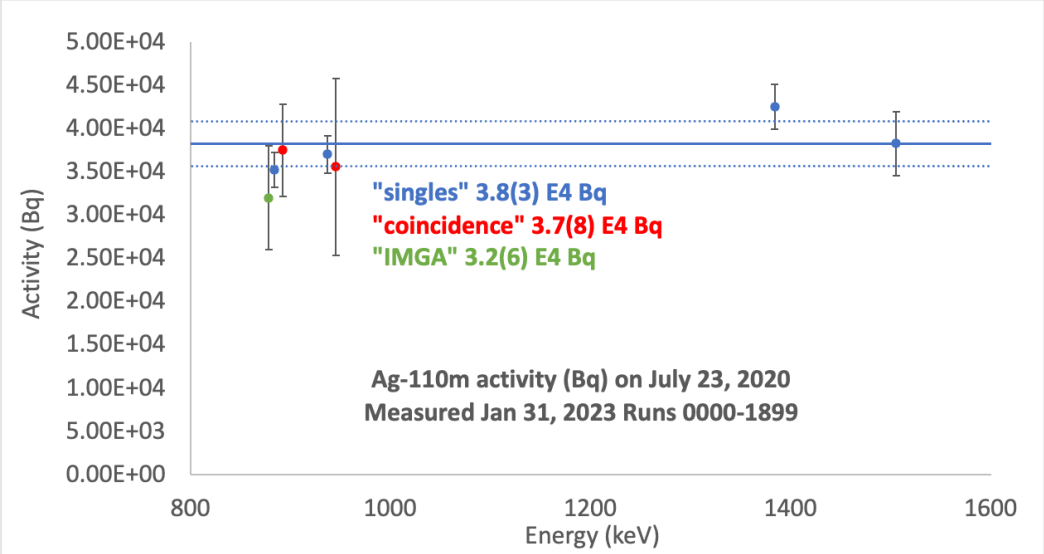

Figure 17. Summary and comparison of results. Reported values are simple averages of results.

The error would be further lowered with longer count times or more detectors counting for the same period. The higher-energy coincidence gates, 1384.3 and 1505.0 keV, were not used as part of this analysis as an examination of the data revealed that the relatively small HPGe crystals did not have sufficient efficiency at high gamma-ray energies to provide statistically significant results during the counting period presented herein. This could be remedied with larger detectors or counting for a longer period.

4. DISCUSSION

4.1 MEASURED INVENTORY AND MDA COMPARISON

Distinguishing the peak from the random background is the largest source of uncertainty in the activity calculation of ^{110m}Ag, raising the MDA. When the counts in the peak are too few with respect to the background in that energy range, ^{110m}Ag activity is no longer extractable from the spectrum. Decreasing

MDA through longer count times is not possible through the traditional method of counting with a single detector whereas increasing count times in coincidence counting increases statistics.

For this measurement, the peak to background ratio for the 884.7 keV peak in the singles spectrum was calculated to be 0.025. For the 884.7 keV peak in the 657.8 keV-gated coincidence spectrum the peak to background ratio was 11.4. This is a factor of 451 improvement in the peak to background ratio and consequentially the MDA. Furthermore, by having at minimum a second detector for coincidence one can determine an empirical in situ detection efficiency which maintains identical geometries and attenuations across measurements [Lauritsen et al. 2016].

With coincidence counting, the MDA becomes a question of how long it is feasible to count a given particle and the cost of an appropriately designed coincidence counting array. An additional benefit of coincidence counting is that many different coincidences may be measured, providing an additional benefit in statistical error reduction.

As an aside, coincidence measurements could prove useful for applications beyond analyses limited by the MDA. The method has implications for the accuracy of any currently employed gamma-ray measurements, including burnup calculations through more precise measurements of cesium and cerium content.

4.2 COINCIDENCE COUNTING FEASIBILITY

The results detailed in Section 3 demonstrate that the challenge proposed in this work is not a question of whether MDA may be lowered; it is instead a question of whether there are resources for an array of the necessary size to count within the desired period. As an example, for AGR program PIE applications involving ^{110m}Ag inventory quantification, a feasible coincidence detection system should not require counting times in excess of 24 h per particle to ensure adequate sample throughput. To achieve the spectra shown in Figure 16, which represents 19 days of coincidence counting with two detectors, an array of eight similarly sized HPGe detectors counting over approximately 16 h would be required. The count period would reduce to approximately 4 h with an array of 16 detectors. Therefore, to maintain a maximum 24 h counting cycle, an HPGe detector array would need at least six detectors of the same crystal size as that used in this experiment to achieve results comparable with IMGA's acquisition data. Improving detector efficiency in a coincidence counting array (e.g., increasing crystal size, reducing sample-to-detector distance) could reduce the required acquisition time. For example, according to Equation 1, doubling the absolute efficiencies of the two HPGe detectors would result in a fourth of the required acquisition time as that of before. This experiment was limited by relatively low detector efficiencies compared with other commercially available HPGe detectors and, as a result, required acquisition times of 1.5 weeks or greater for a single particle measurement. The prescribed acquisition times for this two detector coincidence counting system would not be feasible for AGR PIE schedules. Another possibility would be to provide a mixed array of LaBr and HPGe detectors as described in Sections 1.3 and 2.2. This combination would significantly reduce cost and system complexity and reduce count times. However, the exact number of detectors required to meet the appropriate count time is pending expansion of analysis to include additional results from the counting experiment performed with the array of two HPGE and three LaBr detectors shown in Figure 5.

An HPGe coincidence-counting detector array imposes several limitations regarding irradiated TRISO particle measurements. Fresh particle fuel (i.e., fuel closer to its EOI date) requires the sample-to-detector distance be increased to achieve input count rates suitable for HPGe detectors in a coincidence-counting array. This requirement inherently lowers the detectors' absolute efficiencies and therefore increases the acquisition time needed for a coincidence measurement. Furthermore, as the fuel decays, ^{110m}Ag decays faster relative to longer-lived radioisotopes (e.g., ^{134}Cs, ^{137}Cs, ^{154}Eu) that contribute to a TRISO particle's

long-term radioactivity. This phenomenon would prevent the ability to move the detectors closer to the sample to maintain a similar ^{110m}Ag measurement acquisition time compared with previous measurements that saw a higher ^{110m}Ag activity. However, no appropriate AGR particle fuel was available at the time to measure midlife (i.e., after approximately 3–7 ^{110m}Ag half-lives) ^{110m}Ag activity, so this theory is deduced from previous IMGA measurements and coincidence-counting observations from this experiment.

5. SUMMARY

To test the utility of gamma-gamma coincidence counting for PIE on TRISO fuel, a temporary array of three HPGe detectors was constructed, all collecting data from a single particle of TRISO fuel with a multichannel digital acquisition system. One of the HPGe detectors failed during a power outage and results discussed in Section 3 were limited to coincidence counting with a simple pair of HPGe detectors. The defective third HPGe detector was eventually replaced with three LaBr inorganic scintillators. Data was collected with this expanded five-detector array over a period of two months and analyzed with code written in C++. The results from the simple two-detector array indicate that coincidence measurements could be useful in lowering the MDA of ^{110m}Ag because coincident gamma rays were observed. The activity of ^{110m}Ag was calculated for three different coincident gamma rays, and results are shown in Table 4. Processing of data from the expanded five-detector array is ongoing to optimize the extraction of coincidence events, in addition to exploring various digitizer settings to reduce contributions from time-random background.

The benefit of coincident counting is that it provides a 2–3 orders of magnitude improvement in the MDA, ameliorating the current challenge of ^{110m}Ag lines falling below the random background and becoming unmeasurable. The challenge of coincidence measurements, however, are that they require large, expensive arrays and longer counting times than what is currently required for single-detector measurements. The overall outcome of this experiment is that with coincidence counting, no limitation exists on MDA, and benefits are likely to other objectives such as the accuracy of burnup calculations.

6. REFERENCES

Allmond, James M. 2016. “Investigating Shape Evolution and the Emergence of Collectivity Through the Synergy of Coulomb Excitation and β decay.” *EPJ Web of Conferences* 123: 02006.

Baldwin, Charles A., John D Hunn, Robert N. Morris, Fred C. Montgomery, Chinthaka M. Silva, and Paul A. Demkowicz. 2012. “First Elevated Temperature Performance Testing of Coated Particle Fuel Compacts from the AGR-1 Irradiation Experiment.” *Proceedings of the 6th International Topical Meeting on High Temperature Reactor Technology (HTR2012)*. Tokyo, October 28–November 1, 2012. Also published in *Nuclear Engineering and Design* 271: 131–141.

Drescher, A., M. Yoho, S. Landsberger, M. Durbin, S. Biegalski, D. Meier, and J. Schwantes. 2017. “Gamma-gamma Coincidence Performance of LaBr3: Ce Scintillation Detectors vs. HPGe Detectors in High Count-rate Scenarios.” *Applied Radiation and Isotopes* 122: 116–120.

FDSi Coordination Committee. 2020. “FRIB Decay Station Initiator Proposal.” Oak Ridge: Oak Ridge National Laboratory. https://fds.ornl.gov/wp-content/uploads/2020/09/FDSi-Proposal-May2020.pdf.

Gerczak, Tyler J., John D. Hunn, Robert N. Morris, Fred C. Montgomery, Darren J. Skitt, Charles A. Baldwin, John A. Dyer, and Brian D. Eckhart. 2018. “Analysis of Fission Product Distribution and Composition in the TRISO Layers of AGR-2 Fuel,” *Proc. 9th International Topical Meeting on High Temperature Reactor Technology (HTR-2018).* Warsaw, October 8–10, 2018. Also published in *Nuclear Engineering and Design* 364: 110656.

Gray, Tim J., James M. Allmond, D. T. Dowling, M. Febbraro, T. T. King, S. D. Pain, D. W. Stracener, et al. 2022. "CLARION2-TRINITY: A Compton-suppressed HPGe and GAGG: Ce-Si-Si Array for Absolute Cross-section Measurements with Heavy Ions." *Nuclear Instruments and Methods in Physics Research Section A: Accelerators, Spectrometers, Detectors and Associated Equipment* 1041: 167392.

Gross, Carl J., T. N. Ginter, D. Shapira, W. T. Milner, J. W. McConnell, A. N. James, J. W. Johnson, et al. 2000. "Performance of the Recoil Mass Spectrometer and Its Detector Systems at the Holifield Radioactive Ion Beam Facility." *Nuclear Instruments and Methods in Physics Research Section A: Accelerators, Spectrometers, Detectors and Associated Equipment* 450(1): 12–29.

Hawkes, Grant L. 2021. *AGR-5/6/7 Daily As-Run Thermal Analyses*. ECAR-5633. Idaho Falls: Idaho National Laboratory.

Hunn, John D., Robert N. Morris, Charles A. Baldwin, Fred C. Montgomery, Chinthaka M. Silva, and Tyler J. Gerczak. 2013. *AGR-1 Irradiated Compact 4-4-2 PIE Report*. ORNL/TM-2013/236. Oak Ridge: Oak Ridge National Laboratory.

Hunn, John D., Charles A. Baldwin, Tyler J. Gerczak, Fred C. Montgomery, Robert N. Morris, Chinthaka M. Silva, Paul A. Demkowicz, Jason M. Harp, Scott A. Ploger, Isabella J. van Rooyen, and Karen E. Wright. 2014. "Detection and Analysis of Particles with Failed SiC in AGR-1 Fuel Compacts." *Proceedings of the 7th International Topical Meeting on High Temperature Reactor Technology (HTR-2014)*. Weihai, October 27–31, 2014. Also published in *Nuclear Engineering and Design* 306: 36–46.

Lauritsen, T., A. Korichi, S. Zhu, A. N. Wilson, D. Weisshaar, J. Dudouet, A. D. Ayangeakaa, et al. 2016. "Characterization of a Gamma-ray Tracking Array: A Comparison of GRETINA and Gammasphere Using a ^{60}Co Source." *Nuclear Instruments and Methods in Physics Research Section A: Accelerators, Spectrometers, Detectors and Associated Equipment* 836: 46-56.

Luxium Solutions. *LaBr Scintillation Crystal*. Accessed March 2, 2023. https://www.crystals.saint-gobain.com/radiation-detection-scintillators/crystal-scintillators/lanthanum-bromide-labr3.

Marshall, Douglas W. 2020. *AGR-5/6/7 Fuel Fabrication Report*. INL/EXT-19-53720, Rev. 1. Idaho Falls: Idaho National Laboratory.

Morrison, Lisa. 2015. *Gamma-Gamma Angular Correlations with the GRIFFIN Spectrometer*. PhD dissertation, Department of Physics, Faculty of Engineering and Physical Sciences. Guildford: University of Surrey.

National Nuclear Data Center. *Evaluated Nuclear Structure Data File (ENSDF)*. Brookhaven, Brookhaven National Laboratory. Accessed March 2023. https://www.nndc.bnl.gov/ensdf/.

Pham, Binh T., Joe J. Palmer, Douglas W. Marshall, James W. Sterbentz, Grant L. Hawkes, and Dawn M. Scates. 2021. *AGR-5/6/7 Irradiation Test Final As-Run Report*. INL/EXT-21-64221. Idaho Falls: Idaho National Laboratory.

Sterbentz, James W. 2020. *JMOCUP Physics Depletion Calculations for the As-Run AGR-5/6/7 TRISO Particle Experiment in ATR Northeast Flux Trap*. ECAR-5321. Idaho Falls: Idaho National Laboratory.